

Speckle-Constrained Filtering of Ultrasound Images

Karl Krissian, Ron Kikinis, Carl-Fredrik Westin
Surgical Planning Laboratory
Harvard Medical School
Boston, MA, USA
{karl,kikinis,westin}@bwh.harvard.edu

Kirby Vosburgh
CIMIT
Cambridge, MA, USA
kvosburgh@partners.org

Abstract

Ultrasound images provide the clinician with non-invasive, low cost, and real-time images that can help them in diagnosis, planning and therapy. However, although the human eye is able to derive the meaningful information from these images, automatic processing is very difficult because of the noise and artefacts present in the image. In this work, we propose to extend the current anisotropic diffusion technique to deal with the speckle noise present in the Ultrasound images. To this end, we use a previously derived model of the noise, and we write the restoration scheme as a energy minimization constrained by the noise model and parameters. This approach leads to a new data attachment term whose optimal weight can be automatically estimated.

1. Introduction

Ultrasound is a low cost, non-invasive imaging modality that has proved popular for many medical applications. However, the coherent nature of ultrasound results in images that are corrupted by speckle noise which reduces the utility of ultrasound for less than highly trained users and also complicates image processing tasks such as feature segmentation. Different approaches have been proposed to reduce the speckle, recent works include wavelet-based filtering [5], and modifications of the standard anisotropic diffusion filter [1, 2], but none of them includes an explicit model of the noise distribution as part of the restoration process. We first give a background on the noise properties in ultrasound images, and on the restoration technique that we use for noise reduction. In section 2, we describe the noise-constrained diffusion proposed by Rudin et al. and we extend this approach to deal with the characteristics of speckle noise. In Section 3, our numerical scheme, the main algorithm and the different parameters are presented. Finally, experiments on both a synthetic and a real datasets are de-

scribed, which show the behavior of our method.

1.1. Model of the speckle in ultrasound images

The speckle noise is known to have a Rayleigh distribution. However, the displayed images from the ultrasound device have different properties. One property of the image is the logarithmic compression. The analytic study of log compressed Rayleigh signals in medical ultrasound has been addressed for example in [6, 3]. Loupas [9] shows that the linear relationship between the mean and the standard deviation valid for Rayleigh distributed speckle no longer holds for ultrasound images. Experimental measurements show that displayed ultrasonic images can be modeled as corrupted with signal-dependent noise of the form:

$$u_0 = u + \sqrt{u}n, \quad (1)$$

where u is the original signal, u_0 is the observed signal, and n is a zero-mean Gaussian variable with standard deviation σ_n . In the scope of this work, we use equation (1) as a model to describe the noise in ultrasound images.

1.2. Anisotropic Diffusion

A general expression of the anisotropic diffusion equation can be written as:

$$\begin{cases} u(x, 0) &= u_0 \\ \frac{\partial u}{\partial t} &= \text{div}(\mathbf{F}) + \beta(u_0 - u), \end{cases} \quad (2)$$

where \mathbf{F} is the diffusion flux and β is a data attachment coefficient.

If $\beta = 0$, particular cases of this equation are: 1) the heat diffusion equation $\mathbf{F} = \nabla u$ which is equivalent to a Gaussian convolution. 2) the Perona and Malik equation [13] with $\mathbf{F} = g(\|\nabla u\|)\nabla u$ where g is a diffusion function. This function has the effect of reducing the diffusion for 'high' gradients, based on a *threshold* δ on the norm of the gradient. 3) the matrix diffusion proposed in [17], which

uses a diffusion matrix noted D with a flux $\mathbf{F} = D\nabla u$. The matrix D can be expressed in a diagonal form, with eigenvectors $(\mathbf{v}_0, \mathbf{v}_1, \mathbf{v}_2)$ and eigenvalues $\lambda_0, \lambda_1, \lambda_2$. Then the flux can be expressed as $\mathbf{F} = D\nabla u = \sum_{i=0}^2 \lambda_i u_{\mathbf{v}_i} \mathbf{v}_i$ where $u_{\mathbf{v}_i} = \nabla u \cdot \mathbf{v}_i$ is the first order derivative of the intensity in the direction of \mathbf{v}_i . In this paper, we will adapt for ultrasound a particular case of the matrix diffusion, where the flux is decomposed in the basis of the gradient (\mathbf{v}_0) and the maximal (\mathbf{v}_1) and minimal (\mathbf{v}_2) curvature directions, as proposed in [8]. This diffusion was especially designed to preserve small tubular structures like blood vessels. The gradient and the principal curvature directions are computed on the smoothed image u^* , where the smoothing is obtained by convolution with a Gaussian of standard deviation σ . The principal curvature directions are computed as two eigenvectors of the matrix $PH_\sigma P$ where H_σ is the Hessian matrix of the image u^* and P is the projection matrix orthogonal to the gradient direction, that is $H' = PH_\sigma P$ with $P = I - \left(\frac{\nabla u^*}{\|\nabla u^*\|} \right) \cdot \left(\frac{\nabla u^*}{\|\nabla u^*\|} \right)^t$, where I is the identity matrix in 3D. The eigenvalues of the diffusion matrix are chosen as functions of the first order derivative of the intensity in the corresponding eigenvector direction, and can be written in the form $\lambda_i(u_{\mathbf{v}_i}) = u_{\mathbf{v}_i} \cdot g_i(u_{\mathbf{v}_i})$. The diffusion in the gradient direction, $g_0(x)$, is chosen as Perona and Malik's diffusion function, i.e $g_0(x) = e^{-\frac{x^2}{\delta^2}}$ where δ is a threshold on the intensity derivative in the smoothed gradient direction, and $0 < g_1 \leq g_2 \leq 1$ weight the diffusion in the principal curvature directions.

The data attachment term was first introduced by Nordström [12], who proposed to unify the variational methods of energy minimization [4, 11] with the anisotropic diffusion equation introduced by Perona and Malik. This term allows a convergence of the diffusion scheme to an image that remains close to the initial data. It regularizes the equation, allows to express it as an optimal solution and obviates the need to choose a diffusion time for stopping the equation.

2. Noise-Constrained Diffusion

The data attachment coefficient β can be optimally estimated from the image in the case of Gaussian noise with zero mean and a known standard deviation σ_n as shown in [15]. Note that, if the standard deviation of the noise is not known a priori, it can be estimated from the initial image by selecting a region of interest containing a single structure and estimating its standard deviation. An alternative is also to run the filter twice, using a first estimate of the standard deviation of the noise, and then using the filtered image to obtain a better estimate of σ_n for a second improved restoration. We first describe the technique proposed by Rudin et al. in the case of Gaussian noise, and then we propose an

extension for the noise model in ultrasound images.

2.1. Optimization for a Gaussian noise [15]

Let $u_0(\mathbf{x})$ denote the voxel values of the observed noisy image for $\mathbf{x} = (x, y, z) \in \Omega$; and $u(\mathbf{x})$ denote the desired restored image. The additive Gaussian noise n is given by $u_0(\mathbf{x}) = u(\mathbf{x}) + n(\mathbf{x})$. The idea proposed in [15] is to write the restoration process as a constrained minimization, where the constraint is defined by the characteristics of the noise, in this case its zero mean and its standard deviation σ_n . This minimization is written $\min \int_{\Omega} \|\nabla u\| d\Omega$, with the two constraints:

$$\int_{\Omega} u d\Omega = \int_{\Omega} u_0 d\Omega, \quad \text{and} \quad \frac{1}{|\Omega|} \int_{\Omega} (u - u_0)^2 d\Omega = \sigma_n^2, \quad (3)$$

which means that the white noise n is of zero mean, and has a given standard deviation $\sigma_n > 0$. This second constraint uses a priori information that the standard deviation of the noise n is σ_n . The Euler-Lagrange equations lead:

$$\frac{\partial u}{\partial t} = \text{div} \left(\frac{\nabla u}{\|\nabla u\|} \right) - \lambda(t)(u - u_0) \quad (4)$$

in Ω , and $\frac{\partial u}{\partial n} = 0$ on the boundary of $\Omega = \partial\Omega$. From these equations, the value of the coefficient $\lambda(t)$ is deduced by multiplying (4) by $(u - u_0)$ and integrating by part over Ω : $\lambda(t) = \frac{-1}{\sigma_n^2 |\Omega|} \int_{\Omega} \nabla(u(t) - u_0) \cdot \frac{\nabla u(t)}{\|\nabla u\|} d\Omega$, where $\nabla(u - u_0)$ is the gradient of the difference between the image being restored and the original noisy image, and \cdot denotes the scalar product operator. This gives a dynamic value $\lambda(t)$, which appears to converge as $t \rightarrow \infty$. According to [15], this approach is based on the gradient projection method of Rosen [14]. In this case the diffusion flux \mathbf{F} of equation (2) is the normalized gradient of the image $\mathbf{F} = \frac{\nabla u}{\|\nabla u\|}$, the equation above can be generalized for any diffusion flux, leading $\lambda(t) = \frac{-1}{\sigma_n^2 |\Omega|} \int_{\Omega} \nabla(u - u_0) \cdot \mathbf{F} d\Omega$. This last equation is also equivalent to:

$$\lambda(t) = \frac{1}{\sigma_n^2 |\Omega|} \int_{\Omega} (u - u_0) \cdot \text{div}(\mathbf{F}) d\Omega \quad (5)$$

2.2. Optimization for Speckle Noise

We use equation (1) as a model for speckle noise, where the standard deviation σ_n of the Gaussian noise n is known. Adapting the work of Rudin et al. [15] to this noise model, the constraint given by equation (3) becomes:

$$E_1(u) = \frac{1}{|\Omega|} \int_{\Omega} \frac{(u - u_0)^2}{u} d\Omega = \sigma_n^2, \quad (6)$$

and its gradient is given by $\nabla E_1(u) = \frac{u^2 - u_0^2}{u^2}$, leading:

$$\frac{\partial u}{\partial t} = \text{div}(\mathbf{F}) - \lambda(t) \frac{u^2 - u_0^2}{u^2} \quad \text{in } \Omega \quad (7)$$

and $\frac{\partial u}{\partial n} = 0$ on the boundary of $\Omega = \partial\Omega$. To compute $\lambda(t)$, we multiply equation (7) by $\frac{u-u_0}{u+u_0}u$ and integrate over the Ω . When steady state has been reached, the left side of (7) vanishes, and we have:

$$\lambda(t) = \frac{1}{\sigma_n^2|\Omega|} \int_{\Omega} \frac{u-u_0}{u+u_0} u \cdot \text{div}(\mathbf{F}) \, d\Omega, \quad (8)$$

3. Numerical Scheme

To improve the computation time and stability, we use a stationary iterative scheme for solving the partial differential equation. Other options include adapting the numerical scheme proposed by Weickert [16, 17], or using the conjugate gradient method as proposed in [7]. The image with N points (pixels or voxels), is represented as vector of \mathbb{R}^N , denoted \mathbf{u} . The diffusion equation (4) or (7) is written in the form $\frac{\partial \mathbf{u}}{\partial t} = \mathbf{A} \mathbf{u} - \mathbf{b}$, where \mathbf{A} is a $N \times N$ matrix and \mathbf{b} is a vector of \mathbb{R}^N depending on the initial image u_0 . We are looking for the fixed point of the equation $\mathbf{A} \mathbf{u} = \mathbf{b}$. To this end, we use the Jacobi or the Gauss-Seidel method. The Gauss-Seidel method consumes little memory because it uses the same image for computing and storing the resulting image. The Gauss-Seidel method converges faster than the Jacobi method, but it introduces some asymmetry in the numerical scheme, than can be compensated by alternating two reverse orders of scanning the image. However, because the Gauss-Seidel technique is recursive, it is difficult to parallelize, while the Jacobi technique is naturally structured for parallel implementation. The description and algorithm below apply to both schemes, the only difference being either to use two images u^k and u^{k+1} for the Jacobi method, or to use the same image for the current and the next iteration in the case of the Gauss-Seidel technique. Details of our numerical scheme and implementation are given below. Our equation is expressed as $\text{div}(\mathbf{F}) - \lambda \frac{u^2 - u_0^2}{u^2} = 0$.

3.1. Discretization of $\text{div}(\mathbf{F})$

We discretize the divergence operator, at a given voxel \mathbf{x} :

$$\begin{aligned} \text{div}(\mathbf{F})(\mathbf{x}) &= \sum_{n=0}^2 \frac{\partial F_n}{\partial x_n} \\ &= \sum_{n=0}^2 F_n(\mathbf{x} + \mathbf{dx}_n/2) - F_n(\mathbf{x} - \mathbf{dx}_n/2), \end{aligned}$$

where $\mathbf{F} = (F_0, F_1, F_2)^t$, and $(\mathbf{dx}_0, \mathbf{dx}_1, \mathbf{dx}_2)$ are the unit vectors along each coordinate. In order to simplify, let us consider the first component of \mathbf{F} . As stated in section

1.2, our flux is written $\mathbf{F} = D\nabla u = \sum_{i=0}^2 \lambda_i u_{\mathbf{v}_i} \mathbf{v}_i$, where $(\mathbf{v}_0, \mathbf{v}_1, \mathbf{v}_2)$ are the gradient vector, and the direction of maximal and minimal curvatures computed on the smoothed image. Our diffusion flux is $\mathbf{F} = \sum_{i=0}^2 u_{\mathbf{v}_i} g_i(u_{\mathbf{v}_i}) \mathbf{v}_i$, and each component is $F_n = \sum_{i=0}^2 u_{\mathbf{v}_i} g_i(u_{\mathbf{v}_i}) \mathbf{v}_{in}$ where \mathbf{v}_{in} is the component number n of the vector \mathbf{v}_i . In order to get the central coefficient that applies to $u(\mathbf{x})$, we need to discretize $u_{\mathbf{v}_i} = \nabla u \cdot \mathbf{v}_i$ at the positions $(\mathbf{x} \pm \mathbf{dx}_n/2)_{n \in \{0,1,2\}}$. Let us consider the case $n = 0$. The linear part comes only from the gradient vector ∇u , which is computed at $\mathbf{x} + \mathbf{dx}_n/2$ using the following discretization: $u_x(x+1/2, y, z) = u_{1,0,0} - u_{0,0,0}$, $u_y(x+1/2, y, z) = (u_{1,1,0} + u_{0,1,0} - u_{1,-1,0} - u_{0,-1,0})/4$, and $u_z(x+1/2, y, z) = (u_{1,0,1} + u_{0,0,1} - u_{1,0,-1} - u_{0,0,-1})/4$, with $u_{a,b,c} = u(x+a, y+b, z+c)$. Isolating the term $u_{0,0,0}$ leads:

$$F_0(\mathbf{x} + \mathbf{dx}_0/2) = \alpha_0^+ (u_{1,0,0} - u_{0,0,0}) + \gamma_0^+ \quad (9)$$

$$\text{with } \alpha_0 = \sum_{i=0}^2 g_i(u_{\mathbf{v}_i}) (\mathbf{v}_{i0})^2 \quad (10)$$

$$\text{and } \gamma_0 = \sum_{i=0}^2 (u_y \mathbf{v}_{i1} + u_z \mathbf{v}_{i2}) g_i(u_{\mathbf{v}_i}) \mathbf{v}_{i0} \quad (11)$$

and $\alpha_n^{\pm} = \alpha_n(\mathbf{x} \pm \mathbf{dx}_0/2)$ (same for γ_n^{\pm}). We define in the same manner α_0^- and γ_0^- , which have the same expressions but estimated at $\mathbf{x} - \mathbf{dx}_0/2$ and we define the same variables for y and z components (α_n and γ_n with $n = 1, 2$). The discretization of $\text{div}(\mathbf{F})$ is then written:

$$\text{div}(\mathbf{F}) = R u_{0,0,0} + S \quad (12)$$

$$\text{with } R = - \sum_{n=0}^2 (\alpha_n^+ + \alpha_n^-) \quad (13)$$

$$\begin{aligned} \text{and } S &= \sum_{n=0}^2 [\alpha_n^+ u(\mathbf{x} + \mathbf{dx}_n) \\ &\quad + \alpha_n^- u(\mathbf{x} - \mathbf{dx}_n) + \gamma_n^+ - \gamma_n^-] \quad (14) \end{aligned}$$

3.2. Overall scheme

Thus, we get the following iterative scheme, starting from $u^0 = u_0$:

$$R(u^k) u^{k+1} + S(u^k) - \lambda^k f(u^{k+1}, u_0) = 0 \quad (15)$$

For Gaussian noise, $f(x, y) = x - y$ and the iterative scheme becomes $u^{k+1} = \frac{S(u^k) + \lambda^k u_0}{\lambda^k - R(u^k)}$. In the case of speckle noise, $f(x, y) = \frac{x^2 - y^2}{x^2}$ and u^{k+1} is the real solution to the third order polynomial equation ($R < 0$ because

$\alpha_i^\pm > 0$):

$$X^3 + \frac{(S(u^k) - \lambda^k)}{R(u^k)} X^2 + \frac{\lambda^k u_0^2}{R(u^k)} = 0. \quad (16)$$

This equation has only one real strictly positive solution, because the constant term $\frac{\lambda^k u_0^2}{R(u^k)}$ is strictly negative. By solving this equation instead of using $f(u^k, u_0)$ in equation (15), we considerably improve the stability of the numerical scheme.

Main Algorithm

We can save computation time by storing the values of the coefficients γ_n^+ and α_n^+ and deducing the coefficients γ_n^- and α_n^- from the previous neighbors: $\alpha_n^-(\mathbf{x}) = \alpha_n^+(\mathbf{x} - \mathbf{dx})$. It only requires storing one coefficient for α_0 , one line of coefficients for α_1 and one plane of coefficients for α_2 (and the same for γ_n).

ALGORITHM 1 (ITERATION $k + 1$).

begin

$$\forall(x, y), \quad \alpha_0^- = \alpha_1^-(x) = \alpha_2^-(x, y) = 0$$

$$\forall(x, y), \quad \gamma_0^- = \gamma_1^-(x) = \gamma_2^-(x, y) = 0$$

$$S_\lambda = 0$$

Compute smoothed image $u_\sigma^k = u^k * G_\sigma$

for $\mathbf{x} = (x, y, z) \in \Omega$

for $n \in \{0, 1, 2\}$ and position $\mathbf{x} + \mathbf{dx}_n/2$:

Compute gradient of the current image ∇u^k

Compute gradient ∇u_σ^k and Hessian matrix $H(u_\sigma^k)$

Compute principal curvature directions

Set $(\mathbf{v}_i)_{i \in \{0,1,2\}}$ as gradient and principal curvature directions

Compute α_n^+ and γ_n^+ using (11).

end for

Compute R and S using (13) and (14).

Set $u^{k+1}(\mathbf{x})$ as the real strictly positive solution of equation (16)

Update integral of equation (8) using equation (12):

$$S_\lambda = S_\lambda + (Ru^k + S) \frac{u^k - u_0}{u^k + u_0} \cdot u^k$$

$$\alpha_0^- = \alpha_0^+; \alpha_1^-(x) = \alpha_1^+; \alpha_2^-(x, y) = \alpha_2^+(x, y)$$

$$\gamma_0^- = \gamma_0^+; \gamma_1^-(x) = \gamma_1^+; \gamma_2^-(x, y) = \gamma_2^+(x, y)$$

end for

$$\lambda_{k+1} = \frac{S_\lambda}{\sigma_n^2 |\Omega|}$$

end.

The **parameters** of the algorithm are σ , δ , g_1 , g_2 , the number of iterations, the type of noise (Gaussian or speckle), the standard deviation σ_n of the noise. The value of σ is usually chosen between 0.8 and 1.5 depending on the noise level in the original image. The threshold δ is chosen as low as possible in order to preserve small structures, but still being able to remove the noise. The coefficient of smoothing in the maximal and minimal curvature directions g_1 and g_2 are usually set to 0.1 and 0.5 for angiograms and 1 and 1 for restoration bigger structures. The typical number of iterations used is between 10 and 40 iterations, and

the method either reaches convergence, or small structures start to disappear which means than some of the previous parameters should be decreased. The standard deviation of the noise is estimated automatically by selecting areas inside structures within the original image.

4. Experiments and Results

4.1. Synthetic image

We created a synthetic 3D image representing a Y-junction of a vessel. The main vessel of radius 4 voxels splits into two branches forming an angle of 90 degrees and of radii 2 and 3 voxels. To make the image similar to an ultrasound acquisition, the intensity of the vessel is set to 25 and the intensity of the background is set to 50. The binary image is then convolved with a Gaussian kernel of standard deviation 0.7 in order to simulate partial volume effect, and a multiplicative noise is added following the model of equation (1), with a standard deviation 1 and 2 for the noise, as shown in figure 1. We use the

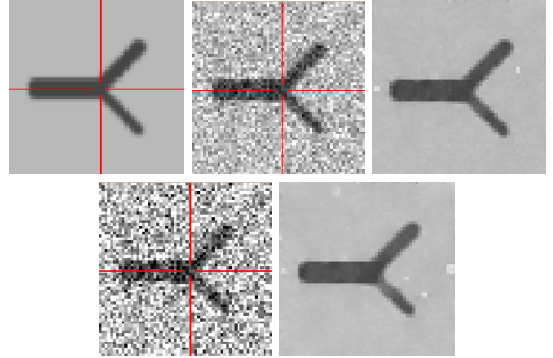


Figure 1. One slice display from the 3D synthetic Y-junction image. From left to right and top to bottom, initial image, initial image with additional noise $\sigma_n = 1$ and the corresponding filtered image, initial image with noise $\sigma_n = 2$ and its filtered result.

following definition of the Signal To Noise Ratio (SNR): $SNR(I_b, I_r) = 10 \log_{10} \frac{var(I_r)}{var(I_b - I_r)}$, where I_r is the image to evaluate, I_b is the initial image without noise, and $var(I)$ denotes the variance of the intensity in the image I . The SNR improved from 1 to 9.8 for the image corrupted by a noise of standard deviation 1, and from 0.3 to 7.1 for the image corrupted by a noise of standard deviation 2. The parameters used in these experiments are: $\sigma = 0.8$, $\delta = 2$, $g_1 = 0.1$, $g_2 = 0.5$, 40 iterations, speckle noise, $\sigma_n = 1$ for the first noisy image; and the same parameters with $\delta = 3$ and $\sigma_n = 2$ for the second noisy image.

4.2. Ultrasound of the liver

A 3D ultrasound of a liver was acquired using a freehand system that consisted of a Lynx ultrasound unit (BK Medical Systems, Wilmington, MA) and a miniBIRD tracking device (Ascension Technology, Burlington, VT). The 3D ultrasound was generated using the Stradx software (Cambridge University, Cambridge, UK). The image dimensions are $201 \times 193 \times 142$ with isotropic voxel resolution. After selecting several areas both in the liver tissue and in the blood vessels, we estimated that, for our noise model, the standard deviation of the noise σ_n is approximately equal to 1. We ran our filter with the following parameters: $\sigma = 0.8$, $\delta = 3$, $g_1 = 0.1$, $g_2 = 0.5$, 30 iterations, speckle noise, $\sigma_n = 1$. The processing time was about 15 minutes on a Pentium Centrino processor running at 1.7 GHz. In the filtered image of figure 2, we can appreciate the noise reduction while most structures are still present in the image. Figure 3 shows, on selected area, the difference between

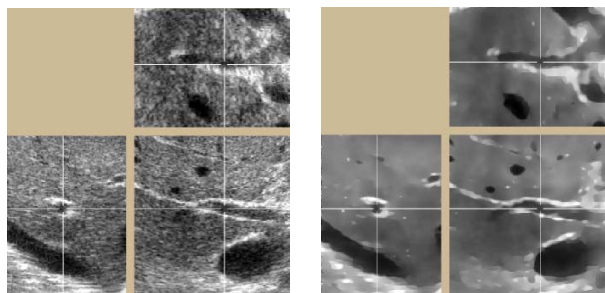


Figure 2. Left, region of interest of a 3D ultrasound dataset of a liver. Right, result of the our filter.

the original and the restored images, and the estimated noise given our noise model. A close inspection should reveal that the latter is more uncorrelated to the different tissues (in this case liver and vessels), which can justify, a posteriori, our multiplicative noise model.

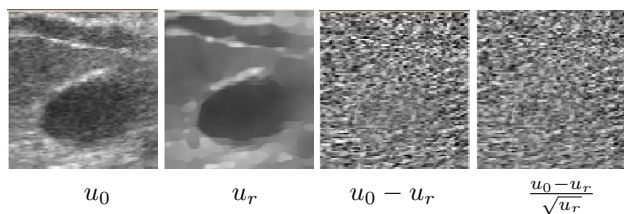


Figure 3. Visual comparison of the noise texture between vessel and liver tissues. From left to right, observed signal, restored signal, their difference, estimated noise.

5. Summary and Conclusions

We presented a new image restoration technique, which takes into account a model of the speckle noise in ultrasound images. This new technique combines an anisotropic diffusion method specially designed for preserving and enhancing small vessel structures [8], with a constrained filtering [15] initially proposed for Gaussian noise, and adapted and extended for the noise characteristics of ultrasound images. We detailed the numerical scheme to allow reproducibility of the results. Our first results are promising. Future work includes evaluating the performance of the filter as a pre-processing tool for automatic segmentation algorithms. We plan in particular to use a level set technique for automatic segmentation of the blood vessels in the liver. Another interesting opportunity is to run intensity correction algorithms like the Expectation-Maximization algorithm proposed in [18], or algorithms based on entropy minimization [10], and ideally to include an intensity correction within our noise reduction technique. Finally, our technique runs in parallel using the Jacobi method, which could lead to real-time noise reduction and segmentation of ultrasound images to better guide interventional and surgical therapies, where the primary skill of the caregiver may not be ultrasound image interpretation.

Acknowledgments

This work was supported by CIMIT grant and NIH P41-RR13218 (NAC).

References

- [1] K. Z. Abd-Elmoniem, A.-B. M. Youssef, and Y. M. Kadah. Real-time speckle reduction and coherence enhancement in ultrasound imaging via nonlinear anisotropic diffusion. *IEEE Trans Biomed Eng*, 49(9):997–1014, Sep 2002.
- [2] S. T. Acton, S. Member, and Y. Yu. Speckle reducing anisotropic diffusion. *IEEE Transactions on Image Processing*, 11(11):1260–1270, nov 2002.
- [3] V. Dutt and J. Greenleaf. Adaptive speckle reduction filter for log-compressed b-scan images. *IEEE Trans. Med. Imaging*, 15(6):802–813, Dec. 1996.
- [4] S. Geman and D. Geman. Stochastic Relaxation, Gibbs Distributions, and the Bayesian Restoration of Images. *IEEE Trans. PAMI*, 6:721–741, 1984.
- [5] S. Gupta, R. Chauhan, and S. Sexana. Wavelet-based statistical approach for speckle reduction in medical ultrasound images. *Med Biol Eng Comput*, 42(2):189–92, Mar 2004gc.
- [6] D. Kaplan and Q. Ma. On the statistical characteristics of the log-compressed rayleigh signals: Theoretical formulation and experimental results. *J. Acoust. Soc. Amer.*, 95:1396–1400, Mar. 1994.

- [7] K. Krissian. A New Variational Image Restoration Applied to 3D Angiographies. In *IEEE W. on Var. and Level Set Meth. in Comp. Vision*, pages 65–72, July 2001.
- [8] K. Krissian. Flux-based anisotropic diffusion applied to enhancement of 3d angiogram. *IEEE Trans. Medical Imaging*, 21(11):1440–1442, Nov. 2002.
- [9] A. Loupas. *Digital image processing for noise reduction in medical ultrasonics*. PhD thesis, University of Edinburgh, UK, 1988.
- [10] J.-F. Mangin. Entropy minimization for automatic correction of intensity nonuniformity. In *IEEE Work. MMBIA*, pages 162–169. IEEE Press, 2000.
- [11] D. Mumford and J. Shah. Boundary detection by minimizing functionals. In *CVPR*, pages 22–26, San Francisco, June 1985. IEEE Comp. Society Press.
- [12] N. Nordström. Biased anisotropic diffusion - A unified regularization and diffusion approach to edge detection. *Image Vision Comput.*, 8(4):318–327, 1990.
- [13] P. Perona and J. Malik. Scale-Space and edge detection using anisotropic diffusion. *IEEE Trans. on Pattern Anal. and Mach. Intel.*, 12(7):629–639, July 1990.
- [14] J. Rosen. "the gradient projection method for nonlinear programming, part ii, nonlinear constraints". *J. Soc. Indust. Appl. Math.*, 9:514–532, 1961.
- [15] L. Rudin, S. Osher, and E. Fatemi. Nonlinear total variation based noise removal algorithms. *Physica D*, 60:259–268, 1992.
- [16] J. Weickert. Recursive separable schemes for nonlinear diffusion filters. In B. ter Haar Romeny, L. Florack, J. Koenderink, and M. Viergever, editors, *Scale-Space Theory in Computer Vision (Scale-Space)*, volume 1252 of *Lecture Notes in Computer Science*, pages 260–271, Utrecht, July 1997. Springer Verlag.
- [17] J. Weickert. *Anisotropic Diffusion in image processing*. Teubner-Verlag, 1998.
- [18] G. W. J. F. Wells WM, Kikinis R. Adaptive segmentation of MRI data. *IEEE Transactions on Medical Imaging*, 15:429–442, 1996.